Core level shifts of undercoordinated Pt atoms

Laura Bianchettin,[1,2] Alessandro Baraldi,[1,2,a)] Stefano de Gironcoli,[3] Erik Vesselli,[1,2] Silvano Lizzit,[4] Luca Petaccia,[4] Giovanni Comelli,[1,2] and Renzo Rosei[1,2]
[1]*Physics Department and Center of Excellence for Nanostructured Materials, Trieste University, Via Valerio 2, I-34127 Trieste, Italy*
[2]*Laboratorio TASC INFM-CNR, S.S. 14 Km 163.5, I-34012 Trieste, Italy*
[3]*Scuola Internazionale Superiore di Studi Avanzati (SISSA) and INFM-CNR DEMOCRITOS National Simulation Center via Beirut 2-4, I-34014 Trieste, Italy*
[4]*Sincrotrone Trieste S.C.p.A., S.S. 14 Km 163.5, I-34012 Trieste, Italy*

(Received 16 November 2007; accepted 15 January 2008; published online 18 March 2008)

We present the results of high-energy resolution core level photoelectron spectroscopy experiments paralleled by density functional theory calculations to investigate the electronic structure of highly undercoordinated Pt atoms adsorbed on Pt(111) and its correlation with chemical activity. Pt4$f_{7/2}$ core level binding energies corresponding to atoms in different configurations are shown to be very sensitive not only to the local atomic coordination number but also to the interatomic bond lengths. Our results are rationalized by introducing an indicator, the effective coordination, which includes both contributions. The calculated energy center of the valence 5*d*-band density of states, which is a well known depicter of the surface chemical reactivity, shows a noteworthy correlation with the Pt4$f_{7/2}$ core level shifts and with the effective coordination. © *2008 American Institute of Physics*. [DOI: 10.1063/1.2841468]

I. INTRODUCTION

The primary role of defect sites in determining the surface chemical reactivity[1–12] is a well-established experimental and theoretical result of surface science with great relevance for the design of new catalysts. In the case of N_2 dissociation on Ru(0001) it has been shown that the activation energy barrier is 1.5 eV higher on the flat surface than that at steps, yielding at 500 K an adsorption rate that is at least nine orders of magnitude lower on the terraces, as the dissociation is largely influenced by the presence of steps.[1] Similar results have been found for NO decomposition on Ru(0001) (Refs. 2 and 3) and for H_2 dissociation on Si(001).[13]

Industrial heterogeneous catalysts, which usually consist of highly dispersed transition metal (TM) nanoparticles exposing different facets and a large number of low-coordinated atoms, may undergo at the typical working temperatures morphological changes that increase the number of surface defects. It has been found that for many surfaces in the 400–1000 K temperature range the density of low-coordinated atoms, such as adatoms, is in the percent range and strongly depends on temperature. Actually, on a surface in thermodynamic equilibrium the thermal adatoms ensemble can be considered as a two-dimensional lattice gas in equilibrium with the step edge.[14] The population of thermal adatoms on Si(001) has been estimated to be 0.01 and 0.03 ML at 920 and 1170 K, respectively, with an adatom formation energy of 0.35 eV.[15] In the case of Ag(110), steps are found to be an efficient adatom reservoir at room temperature and in ultrahigh-vacuum conditions, with a single site detachment rate along the step of 3 atoms/s,[16] which is independent on the step length. It is important to remark that an adatom concentration of a few percent is sufficient to dominate the overall reaction rate in a catalytic process: the low adatom concentration can indeed be compensated by the higher reaction rate due to the lower activation barriers. For instance, it has been found that the first methane dehydrogenation process is highly favorite at the Rh-adatom site on Rh(111) with respect to step or terrace sites[17,18] and that single TM adatoms deposited on oxides can activate the C–H bond scission,[19] the acetylene ciclomerization,[20] and the CO oxidation.[21]

Another relevant contribution determining the chemical reactivity is the surface strain, as demonstrated by experiments and theory. Gsell *et al.*[22,23] found preferential oxygen and carbon monoxide adsorption on the stretched regions obtained through subsurface argon implantation on Ru(0001), while the strong correlation between calculated chemisorption/dissociation energies and surface strain first reported by Mavrikakis *et al.*[24] has been confirmed in more recent investigations.[25–27] The first microscopic evidence of the strain effect on the reaction kinetics has been reported by Wintterlin *et al.*[28] who measured an enhanced NO dissociation probability at the local expanded areas of the Ru(0001) dislocations. In the case of a supported nanoparticle catalyst it has been observed that adsorption on small size clusters can induce a considerable stress in the surface region.[29] In any case, the existence of strain, originated by surface defects or by the interaction with the support, seems to be a general feature of surface catalysts.

In the present paper, we report on the properties of highly undercoordinated Pt atoms, such as adatoms and ad-

a)Author to whom the correspondence should be addressed. Electronic mail: alessandro.baraldi@elettra.trieste.it.

dimers, deposited on Pt(111). By using high-energy resolution core level photoelectron spectroscopy experiments and *ab initio* density functional theory calculations, we have been able to define a reliable indicator that takes into account the effects on surface core level shift (CLS) and the local electronic structure of both coordination and strain. This is important in view of the expected[30–33] strong correlation between surface structure and reactivity.

II. EXPERIMENTAL METHODS

The photoemission experiments were performed at the SuperESCA beamline[34] at the third generation synchrotron radiation source Elettra in Trieste. This beamline is equipped with an ultrahigh-vacuum chamber (base pressure always better than 2×10^{-10} mbar) with standard surface science techniques for sample preparation and characterization and a double pass hemispherical electron energy analyzer with a 96 channel detector.[35]

The Pt(111) single crystal was cleaned by a sequence of Ar^+ sputtering at 300 K, annealing to 1270 K, oxygen treatments in the range of 470–970 K at $p_{O_2}=1\times10^{-8}$ mbar in order to remove carbon and hydrogen reduction to remove residual oxygen traces ($p_{H_2}=5\times10^{-8}$ mbar $T=300$–620 K). Surface cleanness was checked by monitoring the contaminant signals (C1*s*, Si2*p*, S2*p*, and O1*s*). Pt4$f_{7/2}$ core level spectra were acquired at three different photon energies (125, 135, and 155 eV) and a sample temperature of 30 K, with a total energy resolution better than 60 meV. Core level spectra binding energies have been calibrated with respect to the Fermi energy. Pt was deposited on the clean surface using a 99.995% purity Pt filament source, previously cleaned with oxygen and hydrogen cycles.

The photoemission spectra have been fitted using a Doniach-Šunjić (DS) function,[36] even if minor problems can arise, as for Pd,[37] because of the Pt change of the density of states at the Fermi level.[38] Although the DS is calculated with a model density of states of an almost filled rectangular band, this function is commonly used to fit high-energy resolution Pt 4*f* core level spectra measured with synchrotron radiation.[39]

The DS function is a convolution of a Lorentzian distribution (whose full width at half maximum Γ describes the finite lifetime of the excited state) with a singularity function characterized by the α index, which reproduces the asymmetric line shape due to the electronic final-state screening of the core hole. The DS function was convoluted with a Gaussian distribution that takes into account the phonon, inhomogeneous effects, and the instrumental resolution. A linear background was also included in the fit.

III. THEORETICAL METHODS

Theoretical calculations were performed within the density functional theory framework[40,41] using the PBE generalized gradient approximation[42,43] (GGA) as implemented in the Quantum-ESPRESSO open source distribution.[44] The ion cores were described by ultrasoft pseudopotential.[45] The electron wave functions are expanded in a plane wave basis setup to a kinetic cutoff energy of 32 Ry. The (111) surface was simulated by repeating a slab of seven atomic layers and a vacuum region of 10 Å with the adatom or the ad-dimer adsorbed on one side of the slab; in the lateral directions we took a (3×3) in-plane periodicity. The geometry is optimized until the total energy is converged to 10^{-6} Ry and the ionic force components on each atom are smaller than 0.001 Ry/bohr.

Integration of the first Brillouin zone (BZ) was done over a $9\times9\times1$ Monkhorst–Pack grid resulting in 12 special k points in the irreducible wedge[46] for the (1×1) surface unit cell and equivalent k point samplings have been used when dealing with larger supercells; in order to deal with the metallic character of the system and to improve the convergence with respect to the number of k points of the BZ integration, the contribution from each k point is broadened by using a Methfessel and Paxton smearing function[47] of order 1 with a width $\sigma=0.012$ Ry.

In the pseudopotential formalism we used, final-state core level binding energies can be accurately computed by describing the excited atom with a pseudopotential generated in the core-excited configuration. In this formulation the core-level binding energies, including final-state effects, are given by the pseudopotential total energy difference supplemented by an additive constant that can be determined for the isolated atom and cancel out when computing binding energy differences. Initial state contributions can also be extracted by a frozen-density calculation. Isolated Rh* excited atoms are simulated by supercells so as to minimize the interaction of the excited atom with its periodic replicas. We found that a (3×3) in-plane periodicity is sufficient to obtain a very good numerical accuracy (a few meV). The estimated absolute error in the computed surface core level shift is ±30 meV. Details of the method we used can be found in Ref. 48. The partial density of states we calculate is defined as the projection of the density of states onto the atomic wave function ϕ_i^{at}: $n_i=\Sigma_n\int_{\mathrm{BZ}}\delta(E-E_n(\mathbf{k}))|\langle\phi_i^{\mathrm{at}}|\psi_n(\mathbf{k})\rangle|^2d\vec{k}$, where $\psi_n(\mathbf{k})$ is the crystal wave function of the nth band at wave vector $\mathbf{k}$. We define the pth moment of the density of states $n_i(E)$ as $\mu_p=\int\varepsilon^p n_i(\varepsilon)d\varepsilon$; μ_0 and μ_1/μ_0 give the total number of states in the band and the center of gravity position B_d, respectively.

From bulk calculations we obtain an equilibrium lattice constant of 3.99 Å in very good agreement with previous first-principles GGA calculations[49–51] and consistent with the well known GGA bond length overestimation with respect to the experimental value of 3.92 Å.[52] Within the convergence criterion described above, we found a first to second interlayer expansion of 0.9%, comparable with previous predictions.[53]

First, we have investigated the preferred adsorption site for the adatom and addimer because of the two possible stacking in the [111] direction for a face centered cubic (fcc) crystal. For the adatom adsorption, the fcc site resulted to be 180 meV lower in energy than the hcp site, in very good agreement with the previously calculated values of 170 meV (Ref. 54) and 210 meV.[55] Also in the case of the ad-dimer, the fcc configuration is more stable with an energy difference of 240 meV with respect to the hcp configuration (300 meV in Ref. 56). The Pt self-diffusion has been extensively inves-

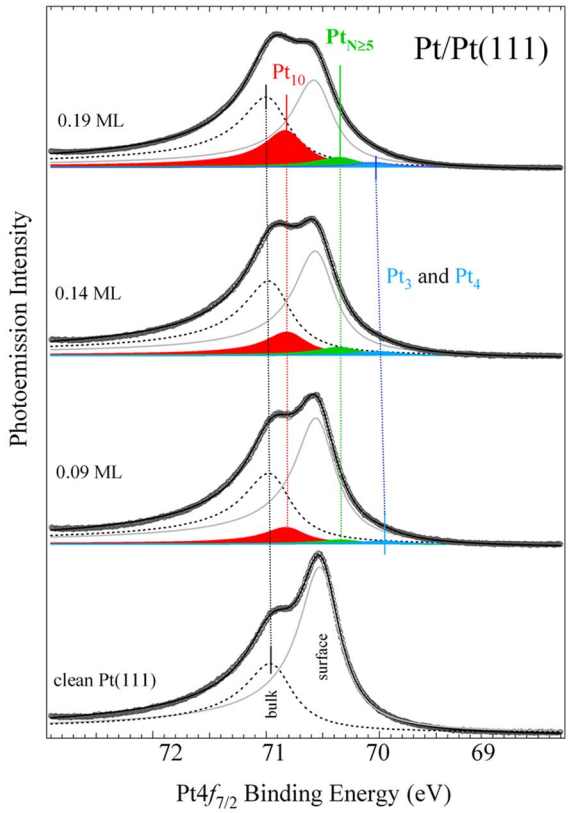

FIG. 1. (Color online) Pt4$f_{7/2}$ core level spectra measured on the clean and differently Pt covered Pt(111) surface. The black dashed line and the gray line indicate the bulk and the clean surface components, respectively, while the blue, green, and red curves correspond to adatoms or ad-dimer $Pt_{3\text{-}4}$, larger cluster Pt_N, and substrate atoms Pt_{10}, respectively. The shown spectra were collected at 125 eV photon energy and at $T=30$ K. The spectra were measured at normal emission.

tigated in the past decade due to the interest in the Pt growth processes; the reported diffusion barrier for the adatom is in the range of 260–330 meV (Refs. 54, 55, 57, and 58) while for the ad-dimer results to be 370 meV.[56,58] It is possible to estimate the activation temperature T of the diffusion process as $T=(E_i/k_B)/\ln(\nu/\Gamma)$, where E is the diffusion energy barrier, ν is the attempt to diffuse frequency $\sim 10^{12}-10^{13}$ s^{-1},[57,58] k_B is Bolzmann's constant and $\Gamma \approx 1$ s^{-1}.[59] For adatoms and ad-dimers on Pt(111), diffusion processes start to become relevant at temperatures above ~ 100 and ~ 150 K, respectively. For this reason, the x-ray photoelectron spectroscopy experiments were performed at 30 K.

IV. EXPERIMENTAL RESULTS

The bottom panel of Fig. 1 shows the Pt4$f_{7/2}$ spectrum from the clean Pt(111) surface: the high binding energy (BE) component at 70.92 eV, indicated with the dashed black line, is originated from the bulk atoms, while the surface component (gray line) is shifted by 420 meV toward lower BE. The best set of line shape parameters corresponding to bulk (B) and surface (S) components, $\Gamma_{B(S)}=0.42(0.38)$ eV, $\alpha_{B(S)}=0.215(0.14)$, $G_{B(S)}=0.09(0.075)$ eV, has been kept fixed for all the series of spectra.

TABLE I. Calculated and experimental core level shifts (meV) relative to the Pt4$f_{7/2}$ bulk core level enrgy position for the different Pt on Pt(111) atomic configurations. The inequivalent Pt atoms are illustrated in Fig. 2. The calculated d-band center shifts ΔB_d are also reported in the right column. For the Pt_9 configuration we have listed only the average CLS value among the inequivalent species.

Structure	Pt atom	Full calc.	Expt.	ΔB_d
Clean	Pt_9	−410	−420	−550
	II-layer	−80		−30
Adatom on (3×3)	Pt_3	−990	−970 to −890	−970
	Pt_9	−340	−440	−520
	Pt_{10}	0		−200
Ad-dimer on (3×3)	Pt_4	−870	−970 to −890	−800
	Pt_9	−400	−390	−490
	Pt_{10}	−170	−120	−290
	Pt_{10}	+30		−150
	Pt_{11}	+190		+80

In Fig. 1, we plot also the Pt4$f_{7/2}$ core level spectra measured after Pt deposition exposures ranging from 20 to 60 s. The unambiguous clean surface component intensity drop and the corresponding intensity increase in the bulk BE region indicate that something is changing on the surface. At first sight new features at low BE are not evident, but an analysis with only two components clearly reveals a low BE shoulder which grows with the deposition time indicative of the presence of a new peak at about 70 eV. After a careful analysis, four distinct components at −120, −420, −590, and −970 meV from the bulk peak can be resolved at low Pt coverage, while at higher Pt coverage there is an upshift of the lowest BE component with a resulting CLS of −890 meV. For high Pt coverage also the bulk peak shifts by about 30 meV toward higher BE. During the fitting procedure only the intensity and BE position are allowed to vary.

In order to estimate the Pt adspecies coverage, we have run a simulation of the deposition process assuming a random distribution model of the Pt atoms adsorbed on the surface, assuming the diffusion process is negligible since the experiment was performed at 30 K: a 20% drop in the Pt clean surface component intensity corresponds to an adspecies coverage of 0.07 ML.

V. THEORETICAL RESULTS AND DISCUSSION

For an unambiguous assignment of the experimental CLS components and for a deep understanding of the electronic properties of the investigated system, we have performed theoretical calculations of the CLS. The experimental (−420 meV) and theoretical (−410 meV) clean surface CLS are in very good agreement. The second layer contribution, which is found in the calculations at +80 meV with respect to the bulk component, seems not to affect in a determinant way the surface CLS (SCLS) evaluation, indicating a low sensitivity to the subsurface contribution in the present experimental conditions.

In Table I, we list the calculated Pt adspecies induced CLS together with the experimental CLS for all the Pt_i

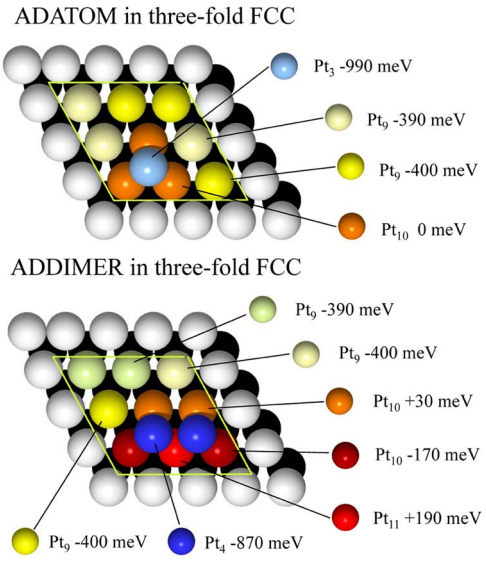

FIG. 2. (Color online) Top view of the structural models for the Pt/Pt(111) surface for the adatom (a) and the ad-dimer (b) configurations. All the inequivalent Pt_i atoms are denoted with different colors. The corresponding calculated CLSs are reported on the right. Note that atoms in different local geometrical configurations can have the same atomic coordination.

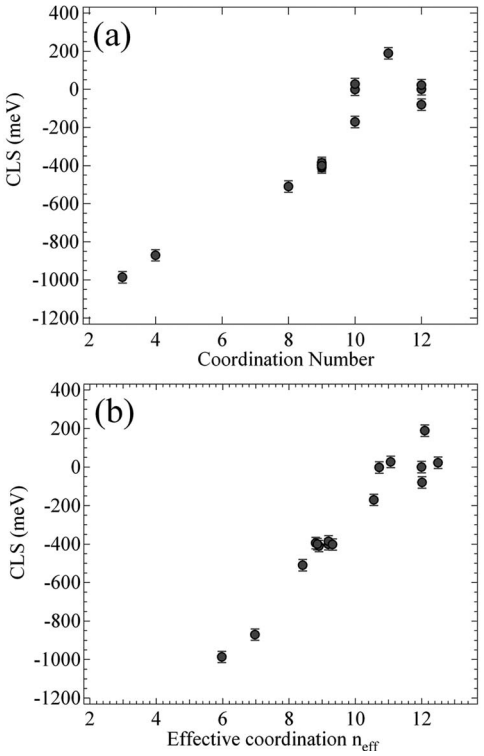

FIG. 3. Calculated CLSs for the homometallic adsorption of Pt on Pt(111) plotted vs the atomic coordination number (a) and vs the effective coordination n_{eff} (b).

$(i=3,4,9,10,11)$ configurations depicted in Fig. 2. From the calculated adatom and ad-dimer CLS (−990 and −870 meV, respectively), we deduce that the experimentally determined shift of the lowest BE component of around +70 meV from low to high Pt coverage originates from the superposition of the two low undercoordinated photoemission contributions; we suppose that, although the enhancement of the ad-dimer population for longer deposition time produces the observed shift, the two peaks are too close in energy and with too low intensity to allow us a proper deconvolution in the data analysis. The experimentally resolved component between the surface and the bulk peak can be assigned to one of the two geometrically inequivalent Pt_{10} substrate atoms (see Fig. 1) bonded to the ad-dimer: indeed, the theoretical calculation shows that these two atoms produce shifts of +30 and −170 meV, respectively, the latter one being closer to the −120 meV component found in the experiments. Although the ad-dimer peak cannot be resolved, the presence of ad-dimers on the surface already from the lowest Pt coverage (0.07 ML) is confirmed by the presence of the −120 meV component. The reasons of the experimentally unresolved Pt_{11} photoemission contribution, which the theory predicts at +190 meV, can be found in (i) line shape and/or background modifications induced by the very close spin orbit splitted component $Pt4f_{5/2}$ BE of 74.29 eV or (ii) in its very low intensity contribution: as reported in Fig. 2, the addition of an ad-dimer yields to four Pt_{10}-type atoms but only to a single Pt_{11}-type substrate atom. In any case we believe that the experimental +30 meV shift of the bulk component mentioned in the Sec. III is just due to the increased Pt_{11} population.

Finally, in the experimental spectra we resolved a further component in the BE range between the Pt_9 and the $Pt_{3,4}$ with an estimated shift of −590 meV, very different with respect to every calculated Pt_i shifts originated by single adatoms or ad-dimers. From the plot of theoretical Pt-induced CLS versus coordination's number, reported in Fig. 3(a), we tentatively assign this contribution to atoms with five or six nearest neighbors that could be obtained from Pt adatom attached to a step edge or from trimers, i.e., cluster of three atoms. Since our sample contains less than 1% of steps, we believe that the major part of that contribution arises from trimers.

We observe that the linear behavior of Fig. 3(a) (linear correlation coefficient $R=0.92$), predicted from fundamental arguments within the tight binding framework, holds only partially: more precisely, the data points relative to low and high coordination numbers do not follow a linear behavior. In analogy with the Rh case,[60] we calculated the effective coordination of the i site defined as $n_{\mathrm{eff}}(i)=\Sigma_i \exp[b(R_{\mathrm{bulk}}-R_{ij})]$, where the sum runs over all the j nearest neighbors, R_{ij} is the distance between atoms i and j, R_{bulk} is the bulk interatomic distance, and b is the decay constant calculated by fitting the isolated atom charge density decay. In this way, it is possible to take into account relaxation effects and assign larger weights to closer atoms. This relation derives from a similar approach used in the embedded atom method,[61–63] which successfully reproduces the metals cohesive energy; in particular, the charge density at each site is approximated by a superposition of atomic charge densities of the nearest neighbor atoms where the charge density distribution is well described by an exponential function in the range of the considered interatomic distance. In Fig. 3(b), the theoretical calculated CLS are plotted against the effective

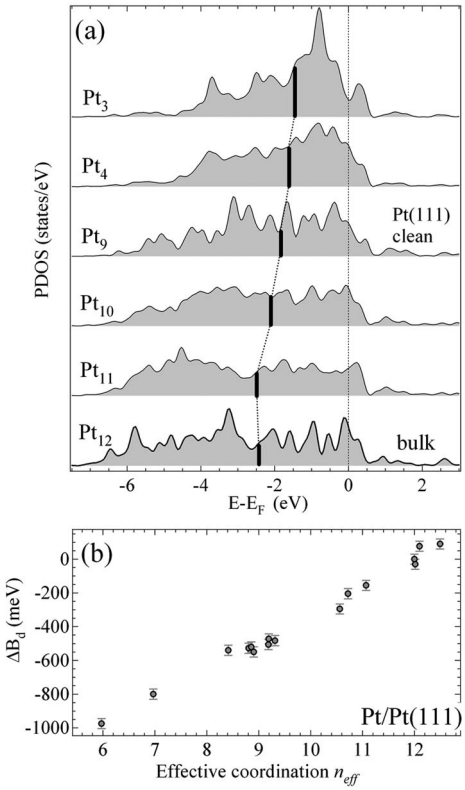

FIG. 4. (a) Projected density of states per Pt atom onto the 5*d* orbital for some of the inequivalent configurations displayed in Fig. 2. In each case we have specified the number of nearest neighbors and the *d*-band center position B_d (tick marks). (b) Calculated shift of the *d*-band center ΔB_d defined as $B_d^{\text{bulk}} - B_d^{\text{surf}}$, vs the effective atomic coordination number n_{eff}.

coordination n_{eff} showing a better overall linear behavior although the slight dispersion (linear correlation coefficient $R=0.96$).

During the past ten years, several experiments have confirmed the relevance of the *d*-band model introduced by Hammer and Nørskov.[30–33] It is nowadays commonly accepted that the surface *d*-band center (B_d) controls adsorbate chemisorption energies and is a good indicator of the surface chemical reactivity since it is correlated with the activation barriers for molecular dissociation, as determined for a wide range of pure and alloyed TM surfaces. More recently theoretical calculations pointed out the influence of low-coordinated atoms on the corners and edges of the nanometer-sized Au nanoparticles which represent the active sites for chemical reactions.[64] Therefore, we calculated the *d*-band center shift corresponding to each individual atomic configuration in order to evaluate its relation with the measured CLS.

Figure 4(a) shows the local electronic density of states projected onto the Pt 5*d* orbital of the Pt_i atoms. As expected, the *d*-band center (thick marks) shifts toward the Fermi level when decreasing the coordination number from 12 (bulk) to 3 (adatom): this is even more evident in Fig. 4(b) where we have plotted the *d*-band center displacement $\Delta B_d = B_d^{\text{bulk}} - B_d^{\text{surf}}$ as a function of the effective coordination n_{eff}. The overall linear behavior suggests that, as for the Rh case,[60] the effective coordination number can be considered as a good indicator of the local chemical properties of Pt atoms, represented by the *d*-band shift ΔB_d. Indeed Fig. 5 points up the linear relationship between the CLS and the *d*-band shift. This result proves that, for the systems where the core-hole screening contributions are not important, the CLSs are good spectroscopic fingerprints of the local chemical reactivity changes.[65,66]

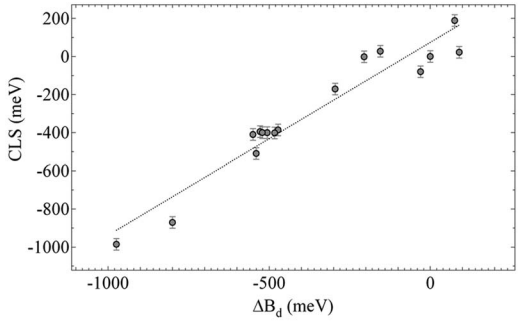

FIG. 5. Calculated CLSs vs the calculated shift ΔB_d for the different Pt on Pt(111) atomic configurations.

VI. CONCLUSIONS

In a recent paper,[60] we have shown the correlation between the CLS and both the effective coordination n_{eff} and the *d*-band center displacement in the case of Rh adsorption on Rh(100) and Rh(111). Here we adopted the same approach extending our investigation to Pt(111). We found that the linear relationship between CLS and n_{eff} holds also for this system. Moreover our experiments confirm that high-energy resolution core level spectroscopy is a valuable tool to investigate highly undercoordinated configurations of TM atoms, preluding possible applications of this method to the study of nanostructured surfaces as in the case of oxide-supported metal nanoclusters.

ACKNOWLEDGMENTS

We acknowledge financial support by the MIUR under the program FIRB 2001 and by Sincrotrone Trieste S.C.p.A. Calculations were performed at the CINECA computing center. Also thanks to INFM-CNR computing grants.

[1] S. Dahl, A. Logadottir, R. C. Egeberg, J. H. Larsen, I. Chorkendorff, E. Törnqvist, and J. K. Nørskov, Phys. Rev. Lett. **83**, 1814 (1997).
[2] T. Zambelli, J. Wintterlin, J. Trost, and G. Ertl, Science **273**, 1688 (1996).
[3] B. Hammer, Phys. Rev. Lett. **83**, 3681 (1999).
[4] Y. Xu and M. Mavrikakis, J. Phys. Chem. B **107**, 9298 (2003).
[5] C. Zhang, Z. P. Liu, and P. Hu, J. Chem. Phys. **115**, 609 (2001).
[6] Z. P. Liu, P. Hu, and A. Alavi, J. Am. Chem. Soc. **124**, 14770 (2001).
[7] Z. P. Liu, S. J. Jenkins, and D. A. King, J. Am. Chem. Soc. **125**, 14660 (2003).
[8] Z. P. Liu and P. Hu, J. Am. Chem. Soc. **125**, 1958 (2003).
[9] T. Zubkov, G. A. Morgan, and J. T. Yates, Jr., Chem. Phys. Lett. **362**, 181 (2002).
[10] F. Buatier de Mongeot, A. Toma, A. Molle, S. Lizzit, L. Setaccia, and A. Baraldi, Phys. Rev. Lett. **97**, 056103 (2006).
[11] J. P. Nielsen and J. K. Nørskov, Top. Catal. **40**, 45 (2006).
[12] B. Hammer, O. H. Nielsen, and J. K. Nørskov, Catal. Lett. **46**, 31 (1997).
[13] P. Kratzer, E. Pehlke, M. Scheffler, M. B. Rascke, and U. Höfer, Phys. Rev. Lett. **81**, 5596 (1998).
[14] N. Lin, D. Payer, A. Dmitriev, T. Strunskus, C. Wöll, J. V. Barth, and K. Kern, Angew. Chem., Int. Ed. **44**, 1488 (2005).
[15] R. M. Tromp and J. P. Toennies, Phys. Rev. Lett. **81**, 1050 (1998).

[16] W. W. Pai, N. C. Bertelt, M. R. Peng, and J. E. Reutt-Robey, Surf. Sci. **330**, L679 (1995).
[17] A. Kokalj, N. Bonini, C. Sbraccia, S. de Gironcoli, and S. Baroni, J. Am. Chem. Soc. **126**, 16732 (2004).
[18] G. Fratesi and S. de Gironcoli, J. Chem. Phys. **125**, 44701 (2006).
[19] S. Abbet, A. Sanchez, U. Heiz, W. Schneider, A. M. Ferrari, G. Pacchioni, and N. Rosch, J. Am. Chem. Soc. **122**, 3453 (2000).
[20] S. Abbet, U. Heiz, H. Häkkinen, and U. Landman, Phys. Rev. Lett. **86**, 5950 (2001).
[21] C. Zhang and P. Hu, J. Chem. Phys. **116**, 4281 (2001).
[22] P. Jacob, M. Gsell, and D. Menzel, J. Chem. Phys. **114**, 10075 (1998).
[23] M. Gsell, P. Jacob, and D. Menzel, Science **280**, 717 (1998).
[24] M. Mavrikakis, B. Hammer, and J. K. Nørskov, Phys. Rev. Lett. **81**, 2819 (1998).
[25] L. A. Kibler, A. M. El-Aziz, R. Hoyer, and D. M. Kolb, Angew. Chem., Int. Ed. **44**, 2081 (2005).
[26] S. Sakong and A. Groß, Surf. Sci. **525**, 107 (2003).
[27] J. R. Kitchin, J. K. Nørskov, M. A. Barteau, and J. G. Chen, Phys. Rev. Lett. **93**, 156801 (2004).
[28] J. Wintterlin, T. Zambelli, J. Trost, J. Greeley, and M. Mavrikakis, Angew. Chem., Int. Ed. **42**, 2850 (2003).
[29] B. Richter, K. Kuhlenbeck, H.-J. Freund, and P. S. Bagus, Phys. Rev. Lett. **93**, 026805 (2004).
[30] B. Hammer, and J. K. Nørskov, Adv. Catal. **45**, 71 (2000).
[31] B. Hammer, Y. Morikawa, and J. K. Nørskov, Phys. Rev. Lett. **76**, 2141 (1996).
[32] J. R. Kitchin, J. K. Nørskov, M. A. Barteau, and J. G. Chen, J. Chem. Phys. **120**, 10240 (2004).
[33] B. Hammer and J. K. Nørskov, Surf. Sci. **343**, 211 (1995).
[34] A. Baraldi, G. Comelli, S. Lizzit, M. Kiskinova, and G. Paolucci, Surf. Sci. Rep. **49**, 169 (2003).
[35] A. Baraldi and V. R. Dhanak, J. Electron Spectrosc. Relat. Phenom. **67**, 211 (1994).
[36] S. Doniach, and M. Sunjic, J. Phys. C **3**, 185 (1970).
[37] S. Surnev, M. Sock, M. G. Ramsey, F. P. Netzer, M. Wiklund, A. Borg, and J. N. Andersen, Surf. Sci. **470**, 171 (2000).
[38] G. K. Wertheim and L. R. Walzer, J. Phys. F: Met. Phys. **6**, 2297 (1976).
[39] J. G. Wang, W. X. Li, M. Borg, J. Gustafson, A. Mikkelsen, T. M. Pedersen, E. Lundgren, J. Weissenrieder, J. Klikovits, M. Schmid, B. Hammer, and J. N. Andersen, Phys. Rev. Lett. **85**, 6102 (2005).
[40] W. Kohn and L. Sham, Phys. Rev. A **140**, 1133 (1965).
[41] P. Hohenberg and W. Kohn, Phys. Rev. B **136**, 864 (1964).
[42] J. P. Perdew, K. Burke, and M. Ernzerhof, Phys. Rev. Lett. **77**, 3865 (1977).
[43] J. P. Perdew, in *Electronic Structure of Solids '91*, edited by P. Ziesche and H. Eshring (Akademie, Berlin, 1991), p. 11.
[44] S. Baroni, S. de Gironcoli, A. Dal Corso, and P. Giannozzi, http://www.quantum-espresso.org
[45] D. Vanderbilt, Phys. Rev. B **41**, 7892 (1990).
[46] H. J. Monkhorst and J. D. Pack, Phys. Rev. B **13**, 5188 (1976).
[47] M. Methfessel and A. T. Paxton, Phys. Rev. B **40**, 3616 (1989).
[48] L. Bianchettin, A. Baraldi, S. de Gironcoli, E. Vesselli, S. Lizzit, L. Petaccia, G. Comelli, and R. Rosei, Phys. Rev. B **74**, 045430 (2006).
[49] N. A. Deskins, J. Lauterbach, and K. T. Thomson, J. Chem. Phys. **122**, 184709 (2005).
[50] A. Kokalj and M. Causà, J. Phys.: Condens. Matter **11**, 7463 (1999).
[51] H. T. Lorensen, J. K. Nørskov, and K. W. Jacobsen, Phys. Rev. B **60**, R5149 (1999).
[52] R. W. G. Wyckoff, *Crystal Structure*, 2nd ed. (Interscience, New York, 1963).
[53] P. J. Feibelman, Phys. Rev. B **56**, 2175 (1997).
[54] G. Boisvert, L. J. Lewis, and M. Scheffler, Phys. Rev. B **57**, 1881 (1998).
[55] P. Feibelman, Phys. Rev. Lett. **81**, 168 (1998).
[56] G. Boisvert and L. J. Lewis, Phys. Rev. B **59**, 9846 (1999).
[57] M. Bott, M. Hohage, M. Morgenstern, T. Michely, and G. Comsa, Phys. Rev. Lett. **76**, 1304 (1996).
[58] K. Kyuno, A. Golzhauser, and G. Ehrlich, Surf. Sci. **397**, 191 (1998).
[59] A. Bogicevic, J. Strömquist, and B. Lundqvist, Phys. Rev. Lett. **81**, 637 (1998).
[60] A. Baraldi, L. Bianchettin, E. Vesselli, S. de Gironcoli, S. Lizzit, L. Petaccia, G. Zampieri, G. Comelli, and R. Rosei, New J. Phys. **9**, 143 (2007).
[61] M. S. Daw and M. I. Baskes, Phys. Rev. Lett. **50**, 1285 (1983).
[62] M. S. Daw and M. I. Baskes, Phys. Rev. B **29**, 6443 (1984).
[63] M. S. Foiles and M. I. Baskes, Phys. Rev. B **33**, 7983 (1986).
[64] B. Hvlbaeb, T. V. W. Janssens, B. S. Clausen, H. Falsig, C. H. Christensen, and J. K. Nørskov, NanoToday **2**, 14 (2007).
[65] J. A. Rodriguez and D. W. Goodman, Science **257**, 897 (1992).
[66] A. Baraldi, S. Lizzit, G. Comelli, M. Kiskinova, R. Rosei, K. Honkala, and J. K. Nørskov, Phys. Rev. Lett. **93**, 046101 (2004).